FORMATION OF FOURIER PHASE SHIFTS IN THE SOLAR Ni I 6768 Å LINE

HARRISON P. JONES*

NASA/Goddard Space Flight Center, Laboratory for Astronomy and Solar Physics, Greenbelt, MD 20771, U.S.A.

(Received 29 September, 1988)

Abstract. A formalism is developed to understand better how Doppler shifts of spectrum lines as inferred from phase shifts in the Fourier transforms of line profiles are related to the underlying velocity structures which they are intended to measure. With a standard model atmosphere and a simplified, quasi-LTE treatment of line formation, the formalism is applied to the Ni I 6768 Å line which has been selected for use with a network of imaging interferometers under development by the Global Oscillations Network Group (GONG) for research in helioseismology. Fourier phase shifts are found to be a remarkably linear measure of velocity even in the presence of gradients and unresolved lateral variations in the assumed velocity field. An assumed outward increase in amplitude of a model oscillatory velocity is noticeably reflected in the center-to-limb behavior of the simulated velocity measure, and a sample model of solar granulation is found to have a strong influence on the formation of the Fourier phase.

1. Introduction

Although detection and measurement of solar velocity fields has an extensive history, the scientific potential of helioseismology for probing the interior of Sun has stimulated renewed interest in developing sensitive imaging 'tachometers' to infer line-of-sight velocities from Doppler shifts of line profiles. The close correspondence between observations and theoretical models reflects the underlying soundness of both the theory and measurement techniques. However, important differences between observers and between observation and theory remain which bear on such fundamental problems in physics and astrophysics as the composition of neutrinos, the internal rotation of the Sun, and convection zone dynamics. More accurate and extensive observations are planned from a ground-based netork being developed by the Global Oscillations Network Group (GONG), by the space-based Michelson Doppler Imager (MDI), and from a variety of individual ground-based instruments. These data will be analyzed to address a broad range of other topics (cf. Libbrecht, 1988, for a recent review of the discipline). The importance of the scientific issues together with the high precision which is required of the data in order to address them implies that the relationship between the velocity field in the outer solar atmosphere and its observational measurement should be thoroughly understood.

Fourier detection of Doppler shifts has become an important method for measuring solar mass motions, and this study accordingly explores how such measurements are affected by non-uniform velocities. Principles of Fourier detection and measurement are

* Mailing address: NASA/GSFC, Southwest Solar Station, c/o National Solar Observatory, P.O. Box 26732, Tucson, AZ 85726, U.S.A.

Solar Physics **120** (1989) 211–234.

described by Evans (1980) and Brown (1984), are incorporated into the currently operating Fourier Tachometer of the High Altitude Observatory and National Solar Observatory, and will be used for the GONG instruments now under development. Doppler shifts are detected in a Fourier Tachometer by an imaging interferometer with fixed path difference between its arms. When solar light is filtered to isolate a single spectrum line and the interferometer image is properly modulated, the final detector output for each pixel can be used to determine the phase of the complex Fourier transform, evaluated at the given path difference, of the spectral profile (intensity as a function of wavenumber). As a consequence of the shift theorem (Bracewell, 1986) the Fourier phase varies linearly with Doppler shifts of the line profile over an unrestricted range of *uniform* velocities and is not sensitive to symmetric variations in line shape. More subtle effects resulting from velocity gradients and spatially unresolved convective motions will be studied here by numerical calculation of the Fourier phase and related transfer quantities in assumed models; no attempt is made to model an actual instrument and its potential sources of signal degradation.

In the presentation to follow, a formalism is developed for a differential 'response function' (Beckers and Milkey, 1975) and a 'formation function' (to be defined below) for understanding the mapping via radiative transfer between assumed velocity structures and the Fourier phase of the emergent profiles. These functions are computed for the 6767.77 Å line of Ni I assuming a standard solar model (VAL-C, Vemazza, Avrett, and Loeser, 1981) and a simple, quasi-LTE treatment of line formation. The Ni line has been chosen for the GONG network and may be used for other future ground-based and spacecraft instruments. Effects of assumed oscillatory and convective velocity structures will be examined, and their implications for high-precision velocity measurements will be discussed. Finally, the numerical techniques used in the computation are presented in the Appendix.

2. Interpreting the Transfer Equation

The equation of radiative transfer,

$$\frac{\partial I}{\partial s}(s, \sigma) = \varepsilon(s, \sigma) - \kappa(s, \sigma) I(s, \sigma), \tag{1}$$

describes the relationship at any point s along a line of sight between the specific intensity I at wavenumber displacement σ from laboratory line-center σ_0, the emission coefficient ε, and the absorption coefficient κ (per unit length). The emergent intensity spectrum seen by an observer at $s = \infty$ is related to the distribution of emissivity and absorption coefficient along the line of sight through the well-known 'formal solution' of Equation (1),

$$I(\infty, \sigma) = \int_{-\infty}^{\infty} \varepsilon(s, \sigma) \exp(-\tau(s, \sigma)) \mathrm{d}s \equiv \int_{-\infty}^{\infty} C(s, \sigma)\, \mathrm{d}s. \tag{2}$$

In Equation (2),

$$\tau(s, \sigma) \equiv \int_{s}^{\infty} \kappa(s', \sigma)\, \mathrm{d}s' \tag{3}$$

is the monochromatic optical path length between a given point along the line of sight and the observer, while $C(s, \sigma)$ is the contribution function for the emergent intensity.

Following Magain (1986), it is useful to combine the transfer equation for continuum and line wavenumbers into a single analog of Equation (1) for line depth,

$$D(s, \sigma) = I_c(s) - I(s, \sigma), \tag{4}$$

where I_c is the continuum intensity. Assuming that I_c is independent of wavenumber and that the line is spectrally isolated, the Fourier phase shifts are formally identical for intensity and depth profiles. However, Fourier transforms of the latter are more accurately computed since, being naturally band-limited in the real domain, its discrete transform is subject to minimal numerical leakage from low frequency components (cf. Brault and White, 1971).

To derive a transfer equation for the line depth, one notes that both absorption and emission coefficients may be separated into line and continuum components so that

$$\varepsilon(s, \sigma) = \varepsilon_c(s) + \varepsilon_l(s, \sigma), \qquad \kappa(s, \sigma) = \kappa_c(s) + \kappa_l(s, \sigma). \tag{5}$$

The transfer equation for continuum wavelengths is

$$\frac{\mathrm{d}I_c}{\mathrm{d}s}(s) = \varepsilon_c(s) - \kappa_c(s) I_c(s); \tag{6}$$

subtracting Equation (1) from Equation (6) and grouping terms according to Magain (1986) gives

$$\frac{\partial D}{\partial s}(s, \sigma) = \varepsilon_D(s, \sigma) - \kappa(s, \sigma) D(s, \sigma), \tag{7}$$

where (suppressing arguments)

$$\varepsilon_D = \kappa_l I_c - \varepsilon_l. \tag{8}$$

Equation (7) is the appropriate transfer equation for D with fixed $I_c(s)$, $\kappa_c(s)$, and $\varepsilon_c(s)$, in addition to many implicit constraints to be discussed below.

The formal solution of Equation (7) is just

$$D(\infty, \sigma) = \int_{-\infty}^{\infty} \varepsilon_D(s, \sigma) \exp(-\tau(s, \sigma))\, \mathrm{d}s \equiv \int_{-\infty}^{\infty} C_D(s, \sigma)\, \mathrm{d}s. \tag{9}$$

Loosely speaking, the emergent radiation originates from, or is formed, along those portions of the line of sight where the contribution function is appreciable. Since the contribution function for the specific intensity is intrinsically positive, its normalized statistical moments (e.g., mean and standard deviation) can be used to describe the location and extent of the region of formation more compactly. Similarly, the variation of C_D along the line of sight indicates where line depth is formed. However, since at any point along the line of sight a spectrum line may be either in absorption or emission with respect to the local continuum intensity, the contribution function for line depth may be positive or negative, and its description by statistical moments should be regarded cautiously.

There appears to be lingering semantic controversy concerning which of many different expressions for contribution functions are valid (cf. Caccin *et al.*, 1977; Magain, 1986). The procedure outlined by Magain is to write a 'transfer' equation of form (1) for the desired quantity, identify its emission and absorption terms, and proceed by analogy with Equations (2) and (3) to identify the 'effective' absorption coefficient, optical path length, and contribution function. Magain claims that proper separation of functions which are dependent (intensity analogues) from those which are independent (absorption and emission analogues) leads to a unique form for the contribution function for line depth. However, although that separation is used in this paper for the case of line depth, a different general view of the transfer equation and its constituent functions is taken, and subsequent derivations for functions describing formation of Fourier phase are not in strict accordance with this seemingly straightforward algorithm.

In general, not even the specific intensity truly 'obeys' a transfer equation; the emission and absorption coefficients depend upon the specific intensity explicitly through stimulated emission and implicity through the equilibrium equations for the ion populations. Even the continuum radiation in LTE is not strictly separable from line formation when one considers the dynamical state and energy balance of the atmosphere (e.g., the effect of line blanketing on radiative equilibrium). One generally *forces* more exact statistical descriptions of quantum mechanical interactions between radiation and matter into the form of Equation (1) (which was originally derived on *phenomenological* grounds) by masking nonlinear and implicit dependencies through suitable definitions of the absorption and emission coefficients. What one calls dependent and independent is tantamount to specifying how these dependencies, both implicit and explicit, are to be constrained – a complete integration path in both geometric and function space must be specified. Thus the transfer equation is not viewed here as a fundamental relation to be solved for a dependent function in terms of known independent ones but as a readily computable mapping between functions which are subject to many additional conditions and whose dependence or independence is thus to be decided according to the situation at hand. In most astrophysical applications, as in this paper, a completely general specification of constraints is sufficiently complicated that it is established (if at all) by context rather than notation.

Another tool for exploring the structure of the formal solution to the transfer equation is the differential 'response function'. In the present case, the line depth depends on the

projected line-of-sight distribution of velocity $v(s)$, and a change δD induced by a distribution of changes $\delta v(s)$ can be expressed in the form

$$\delta D(s, \sigma) \equiv \int_{-\infty}^{s} R_{D:v}(s, s', \sigma) \delta v(s') \, ds', \tag{10}$$

where R is the response function. Subsequent references will be only to response functions for emergent quantities, and the first spatial argument will be suppressed ($R(s', \sigma) \leftrightarrow R(\infty, s', \sigma)$). The response function is evaluated for fixed emission, absorption, line depth, and velocity; again, a complete set of constraints must be specified, but contextual ambiguities are less troublesome since R describes a differential response in much the same way as a partial derivative.

Since the oscillatory velocity of the Sun is the superposition of $\sim 10^7$ low-amplitude modes, the product of the response function and the line-of-sight projection of a velocity eigenfunction shows how the emergent quantity is sensitive to that mode. Any change in the response function with *total* velocity or position on the disk implies that the linearity of velocity superposition on the Sun will not be preserved in its measurement, and the subsequent decomposition of the data into observed eigenmodes will be correspondingly distorted.

The absorption and emission in the observer's frame are related to that in the local rest frame of the gas through the Doppler shift (assuming $v/c \ll 1$) by

$$\varepsilon(s, \sigma) = \varepsilon_0(s, \sigma + \sigma_0 v(s)/c) \tag{11a}$$

and

$$\kappa(s, \sigma) = \kappa_0(s, \sigma + \sigma_0 v(s)/c), \tag{11b}$$

where motions away from the observer have positive velocity. If the velocity is constant along the line of sight, the emergent intensity is similarly Doppler-shifted, and its Fourier phase is simply proportional to the velocity. Note that constraints on functional dependencies within the model atmosphere are already implicit in Equations (11); that is ε_0 and κ_0 refer to the emission and absorption coefficient within an atmosphere at rest but with identical thermal and density structure as well as the same distribution of level populations even though all of these quantities are in principle interdependent.

To derive the response function for velocity-induced changes in line depth, note that the differential changes in emission and absorption coefficients can be derived from Equations (11) as

$$\begin{aligned} \delta\varepsilon_D(\sigma, s) &= \frac{\sigma_0}{c} \delta v(s) \frac{\partial \varepsilon_D}{\partial \sigma}(\sigma, s), \\ \delta\kappa(\sigma, s) &= \frac{\sigma_0}{c} \delta v(s) \frac{\partial \kappa}{\partial \sigma}(\sigma, s). \end{aligned} \tag{12}$$

Since

$$\frac{\partial \kappa}{\partial \sigma} D = \frac{\partial}{\partial \sigma}(\kappa D) - \kappa \frac{\partial D}{\partial \sigma},$$

the differential of the transfer equation (7) can be written as

$$\frac{\partial \delta D}{\partial s} = \frac{\sigma_0}{c} \delta v \left[\frac{\partial}{\partial \sigma}(\varepsilon_D - \kappa D) + \kappa \frac{\partial D}{\partial \sigma} \right] - \kappa \delta D . \tag{13}$$

Substitution from Equation (7) for $\varepsilon_D - \kappa D$ in Equation (13) then leads to

$$\left(\frac{\partial}{\partial s} + \kappa \right) \delta D = \frac{\sigma_0}{c} \delta v \left(\frac{\partial}{\partial s} + \kappa \right) \frac{\partial D}{\partial \sigma} . \tag{14}$$

If one multiplies Equation (14) by $\exp(-\tau(s, \sigma))$ and integrates the result along the line of sight, one obtains an expression in the form of Equation (10) with

$$R_{D:v}(s, \sigma) = \frac{\sigma_0}{c} \frac{\partial}{\partial s} \left[\exp(-\tau(s, \sigma)) \frac{\partial D}{\partial \sigma}(s, \sigma) \right]. \tag{15}$$

Although a similar relation has been used by Jones (1985) for the case of magnetic fields, it is more common (see, for example, Beckers and Milkey, 1975) to express response functions entirely in terms of the contribution function. However, the form used here is in keeping with the view of the transfer equation discussed earlier, and experience has shown that Equation (15) leads to accurate numerical algorithms with simple quadratures and interpolation.

3. Formation of Fourier Phase

The centered transform of the line depth for interferometer path difference x may be written as

$$\tilde{D}(s, x) = \int_{-\infty}^{\infty} \exp(-2\pi i x \sigma) D(s, \sigma) \, d\sigma . \tag{16}$$

From the phase of the emergent $\tilde{D}$ one infers the line of sight velocity to be

$$\zeta(x) = \zeta_0 \tan^{-1}[\mathrm{Im}\tilde{D}(\infty, x)/\mathrm{Re}\tilde{D}(\infty, x)], \tag{17}$$

where $\zeta_0 = c/(2\pi\sigma_0 x)$. It is convenient to separate the line-depth profile into symmetric and antisymmetric components so that the complex transform may be written in terms of real quantities. This is simply accomplished by the transformation

$$p(s, \sigma) = \tfrac{1}{2}(D(s, \sigma) + D(s, -\sigma)), \qquad q(s, \sigma) = \tfrac{1}{2}(D(s, \sigma) - D(s, -\sigma)) \tag{18}$$

and its inverse

$$D(s, \sigma) = p(s, \sigma) + q(s, \sigma), \qquad D(s, -\sigma) = p(s, \sigma) - q(s, \sigma). \tag{19}$$

Then the real and imaginary components of Equation (16) can be written as

$$\begin{aligned} \operatorname{Im} \tilde{D}(s, x) &= \int_0^\infty -\sin(2\pi x \sigma) q(s, \sigma)\, \mathrm{d}\sigma \equiv \tilde{q}(s, x), \\ \operatorname{Re} \tilde{D}(s, x) &= \int_0^\infty \cos(2\pi x \sigma) p(s, \sigma)\, \mathrm{d}\sigma \equiv \tilde{p}(s, x). \end{aligned} \tag{20}$$

By taking the transform of the formal solution (9) for the transfer equation for line depth and interchanging order of integrations, one can use Equation (17) to write

$$\zeta_0 \tan(\zeta/\zeta_0) = \int_{-\infty}^{\infty} [\zeta_0 \tilde{C}_q(s, x)/\tilde{p}(\infty, x)]\, \mathrm{d}s \equiv \int_{-\infty}^{\infty} C_\zeta(s, x)\, \mathrm{d}s, \tag{21}$$

where, corresponding to definitions (18) and (20),

$$\begin{aligned} C_p(s, \sigma) &= \tfrac{1}{2}(C_D(s, \sigma) + C_D(s, -\sigma)), \\ C_q(s, \sigma) &= \tfrac{1}{2}(C_D(s, \sigma) - C_D(s, -\sigma)), \end{aligned} \tag{22}$$

and

$$\tilde{C}_D = \tilde{C}_p + i\tilde{C}_q. \tag{23}$$

C_ζ, with units of velocity per unit path length, will be called a phase 'formation' function to distinguish it from a contribution function to which it is in some ways analogous. Like a contribution function, C_ζ indicates where Fourier phase is 'formed' along the line of sight and, through its dependence on $\tilde{C}_q$, is affected both by local conditions and by the material intervening between a local volume and the observer. It is in this sense that the calculations to follow will be used to gain insight into the effects of internal velocity fields on the emergent phase. However, no attempt has been made to force the Fourier transform of the transfer equation into a transfer equation for phase itself, which, after all, is neither emitted not absorbed by the constituent gas. Thus, the simple physical interpretation (the amount of specific energy emitted from a given interval on the line of sight which reaches the observer after absorption by intervening matter) associated with the ordinary contribution function does not extend to the phase formation function. Moreover, in keeping with our relaxed view of the transfer equation and its constituent functions, C_ζ is computed for fixed p and thus 'confuses' independent and dependent functions in the sense of Magain. Finally, ζ is not linearly related to C_ζ.

From the definitions (18) for p and q, one may show that

$$R_{p:v}(s, \sigma) = \tfrac{1}{2}[R_{D:v}(s, \sigma) + R_{D:v}(s, -\sigma)] ,$$
$$R_{q:v}(s, \sigma) = \tfrac{1}{2}[R_{D:v}(s, \sigma) - R_{D:v}(s, -\sigma)] . \tag{24}$$

The response function relating changes in ζ to changes in distribution of velocity follows by taking the differential of Equation (17) and noting the definitions (20). The result is

$$R_{\zeta:v}(s, x) = \zeta_0(\tilde{p}(\infty, x)\tilde{R}_{q:v}(s, x) - \tilde{q}(\infty, x)\tilde{R}_{p:v}(s, x))/|\tilde{D}(\infty, x)|^2 , \tag{25}$$

where

$$\tilde{R}_{D:v}(s, x) = \tilde{R}_{p:v}(s, x) + i\tilde{R}_{q:v}(s, x) . \tag{26}$$

The numerical methods used to compute C_ζ and $R_{\zeta:v}$ along with related transfer quantities are presented in the Appendix.

4. Emission and Absorption Coefficients

The 6768 Å line is produced by transitions between the a^1S_1 (lower level) and $z^3P_3^0$ levels of Ni I and is the sole permitted transition of multiplet number 57 (of 296) in the Moore (1959) multiplet tables. The lower level is metastable in the sense that only dipole forbidden radiative transitions to lower energy states can occur; the upper level couples to numerous other states of both higher and lower energies. While this intricate atomic structure makes detailed studies difficult, numerical techniques are now available for multi-level, non-LTE analyses of appropriate complexity. However, applying the methods is still non-trivial, and simply collecting the best available atomic data to begin such a venture is a major task. In fact, non-LTE calculations are now being made by Rutten *et al.* (1989), and it is hoped that these will improve the realism of the modeling. However, to provide early input for instrumental considerations (including line selection) a quasi-LTE interim method for synthetically modeling observed spectra was developed (Jones, 1987) and is used for computing the response and phase-formation functions reported here.

Pressure, density (electron, neutral hydrogen, total), electron temperature, microturbulent velocity, and H^- departure coefficients are taken from the VAL-C model atmosphere (Vernazza, Avrett, and Loeser, 1981). Needed oscillator strengths are taken from Wiese and Martin (1980) and Corliss and Bozman (1962), a standard solar Ni abundance from Allen (1974) is used, and the usual approximations are made for Van der Waals and Stark broadening in determining the Voigt damping parameter (Mihalas, 1978).

To improve the fit of computed profiles to observations made with the National Solar Observatory's Fourier Transform Spectrometer on Kitt Peak (Hubbard, 1987; private communication) several additional approximations are made. The proportionality constant for the line center absorption coefficient (i.e., the product of the oscillator strength, the Ni abundance, and the departure coefficient of the lower level relative to Ni II) are

reduced by a factor of ~ 2 – an approximation qualitatively consistent with non-LTE 'overionization' of Ni I as reported by Rutten *et al.* (1989). The variation of the line source function with height, h, is specified in terms of the Planck function, B_ν, by

$$S_l(h) = \begin{cases} B_\nu(h^*), & h > h^*, \\ B_\nu(h), & h < h^*, \end{cases} \tag{27}$$

where τ_l is the monochromatic optical depth at line center and $\tau_l(h^*) \equiv 1$.

The above form for the line source function (here for intensity, not line depth) improves the fit of the computed center-to-limb behavior to observation and can be regarded as a crude scaling-law approximation to represent mild non-LTE excitation effects in the outer layers of formation. These are qualitatively suggested by the comparatively featureless appearance of spectroheliograms taken in the Ni line (Duvall, 1987; private communication) which implies that the line formation is partially decoupled from spatial variations in the thermodynamic state of the atmosphere.

The above model of line formation for the Ni line is far from definitive and was intended to be an interim procedure for early and timely investigations associated with the GONG project. It has the virtue of being in reasonable accord with observation and is simple enough to allow efficient experimentation with velocity fields which affect the emergent intensity primarily through the influence of Doppler shifts on optical depth and relative weighting between line and continuum emission coefficients. In any case, the formalism for investigating phase formation can equally well be applied to non-LTE calculations and this will presumably be accomplished as the results of Rutten *et al.* (1989) and perhaps others become available.

5. Results

Phase formation and response functions have been calculated using the VAL-C atmosphere and the preliminary model of line formation discussed in the previous section. All the calculations reported here are for an interferometer path difference of $x = 1.5$ cm (see Equation (16)), the value expected to be incorporated in the GONG instruments.

5.1. Oscillatory velocity stratification

To represent the total velocity in a typical five-minute oscillation, an instantaneous stratification is introduced which varies as the reciprocal 0.3 power of density (Mein, 1966). The amplitude of this velocity field is carried as a parameter which can be varied, for example, as a function of time to simulate an oscillation period; the velocity is normalized to a value at $\tau_{5000} = 1$ of $v_0 = 0.33$ km s^{-1} for most of the results reported here. As shown in Figure 1, this oscillatory velocity is of the same order as, but less than, both the total and thermal Doppler broadening velocities of the model except in its outer layers. Since the rapid outward decrease of line absorption coefficient limits the height where velocity fields appreciably affect phase formation, no attempt has been made to

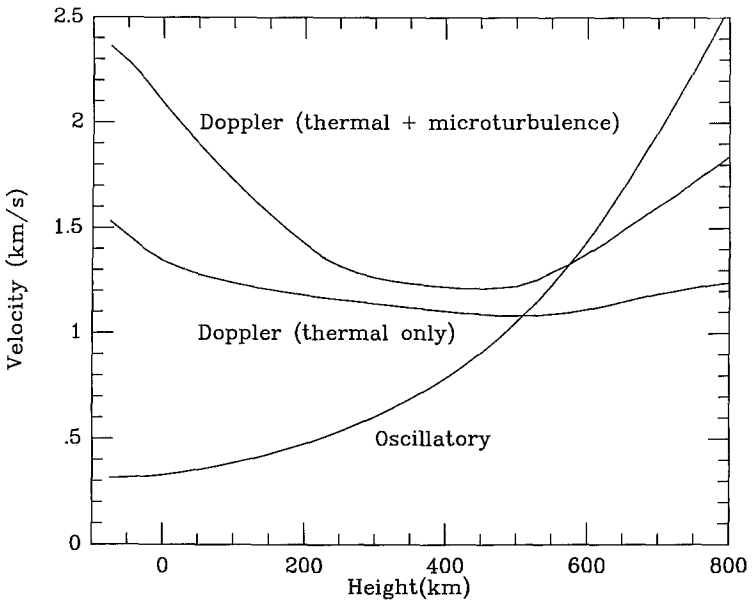

Fig. 1. Broadening (VAL-C) and oscillatory velocities as a function of height.

model the eventual saturation of amplitude growth with height. In the absence of other information, one would expect from Figure 1 that results based on Taylor expansions in oscillatory over Doppler broadening velocities should be qualitatively correct but might show appreciable quantitative differences compared to more precise computations. In fact, as discussed below, a number of approximate expectations are fulfilled in more accurate computations with unexpected quantitative precision.

Figure 2 shows for reference the variation of the line-depth contribution function with height at disk center for several values of wavenumber and zero oscillatory velocity. Note the rather broad height distribution, particularly at line center. Figures 3(a) and 3(b) show the computed response and phase formation functions for the above model at several values of heliocentric angle $\theta \equiv \cos^{-1}\mu$ with a downward (positive) oscillatory velocity at the nominal amplitude.

Recall that the response function, $R_{\zeta:v}$ (here expressed per unit *height* interval rather than path length) describes the change in Fourier phase shift (in velocity units) induced by a unit change in *line-of-sight* velocity. An important result to emerge from these calculation (see below for further discussion) is that $R_{\zeta:v}$ depends only weakly on the actual velocity in the model. Thus, in Figure 3(a), one sees primarily the effects of the outward shift in the mapping between optical path length and height as one proceeds from center to limb. The amplitude of the response function does not change much, and the changes which are apparent reflect the concentration of $R_{\zeta:v}$ into narrower height domains toward the limb.

On the other hand, the phase formation function (roughly the product of the response function and the oscillatory velocity) as shown in Figure 3(b) depends directly on the

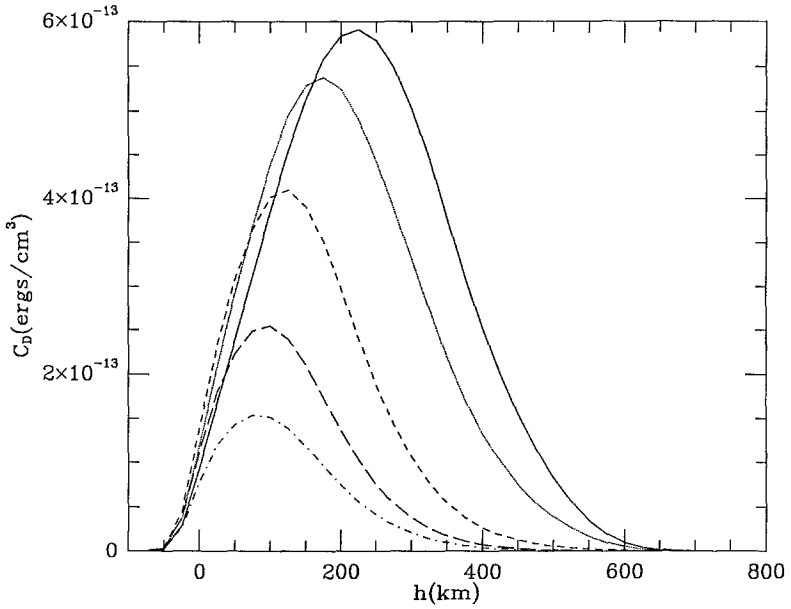

Fig. 2. Monochromatic contribution functions for line depth in the VAL-C atmosphere at disk center for several positions in the line. Line center ($\sigma = 0$), solid; $\sigma = 0.09$ cm^{-1}, dots; $\sigma = 0.18$ cm^{-1}, short dashes; $\sigma = 0.27$ cm^{-1}, long dashes; $\sigma = 0.36$ cm^{-1}, dot-dash.

total projected line-of-sight velocity in the model and thus decreases in amplitude from center to limb for vertical motions. The response function peaks occur lower in the atmosphere than the phase formation function because the assumed oscillatory velocity increases outward. When compared to the monochromatic contribution function at disk center as shown in Figure 2, the response function varies with height in much the same way as the contribution function as a wavenumber displacement of 0.09 cm^{-1}, presumably reflecting the frequency weighting in the Fourier transform. The phase formation function at disk center, however, peaks slightly higher than the line-center contribution function, again showing the effect of the outward increase in oscillatory velocity.

For a given temperature-density structure, the response function is remarkably independent of the assumed oscillatory velocity amplitude over a range of velocities far exceeding measured solar values. The precision of this independence, which was sufficiently unexpected to prompt several checks for software errors, is compactly viewed in Figure 4 where the final Fourier-phase velocity, ζ, is shown as a function of oscillatory velocity amplitude, v_0, at $\tau_{5000} = 1$ for several values of μ. The fractional variation of ζ is less than about one part in a thousand over a range of v_0 exceeding expected solar amplitudes by a factor of four. The linear dependence of Fourier phase shift with *uniform* velocity along the line of sight is an important reason for selecting Fourier phase detection as a means for measuring Doppler shifts. It is satisfying that this linearity extends to non-uniform velocities with high enough precision that resultant waveform distortions introduced into helioseismology observations are negligible for an error budget well below the 1 m s^{-1} level.

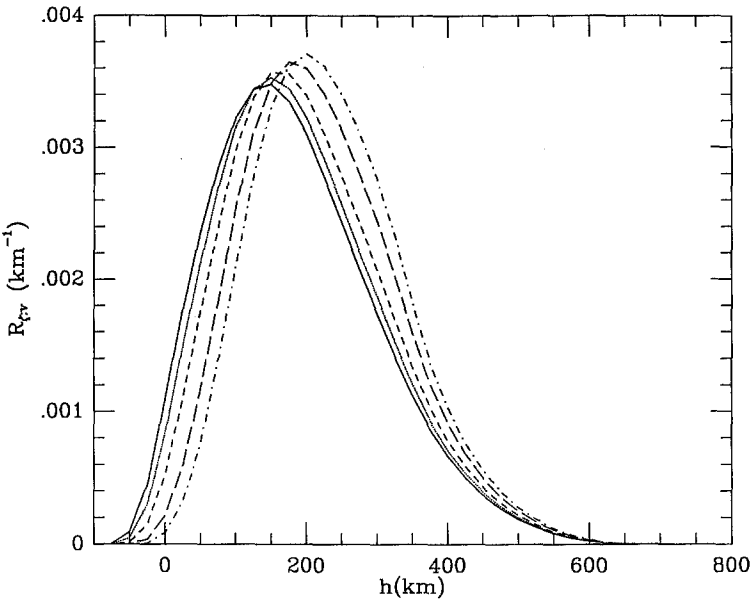

Fig. 3a.

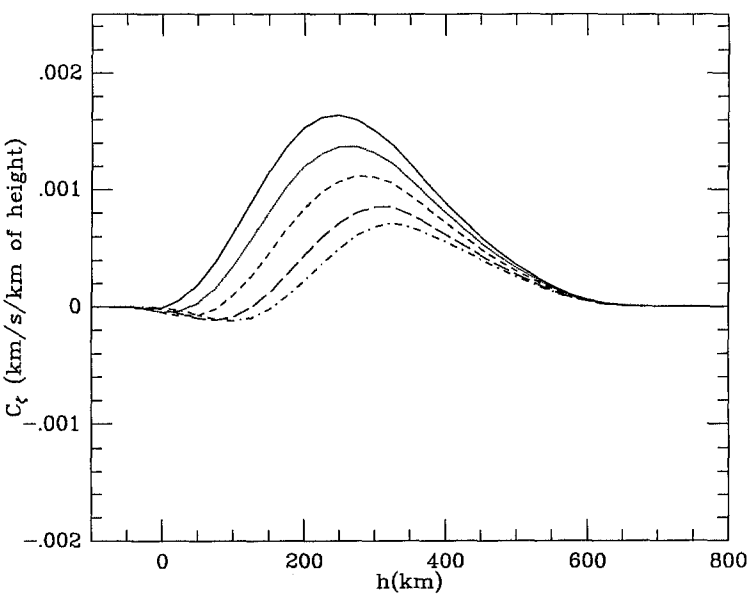

Fig. 3b.

Fig. 3. (a) Response function as a function of height at several disk positions: $\mu = 1.0$, solid; $\mu = 0.8$, dots; $\mu = 0.6$, short dashes; $\mu = 0.4$, solid dashes; $\mu = 0.2$, dot-dash. (b) Phase formation function vs. height at several disk positions. Currents labeled as in (a).

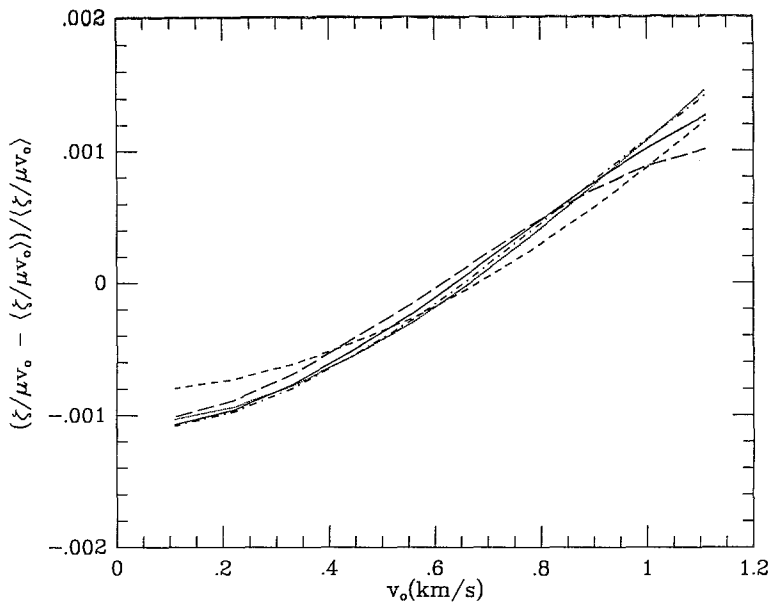

Fig. 4. Relative variation of Fourier-shift velocity (ζ) vs. oscillatory velocity amplitude at $\tau_{5000} = 1$ for several values of μ. Dashed patterns as in Figure 3(a).

On the other hand, there is a slight but noticeable dependence of Fourier phase shift with center-to-limb position, in the sense that velocities near the limb are overestimated. This effect can be seen in Figure 5, where the ratio of ζ to the projected line-of-sight velocity at $\tau_{5000} = 1$ is plotted as a function of μ, and is a natural consequence of the

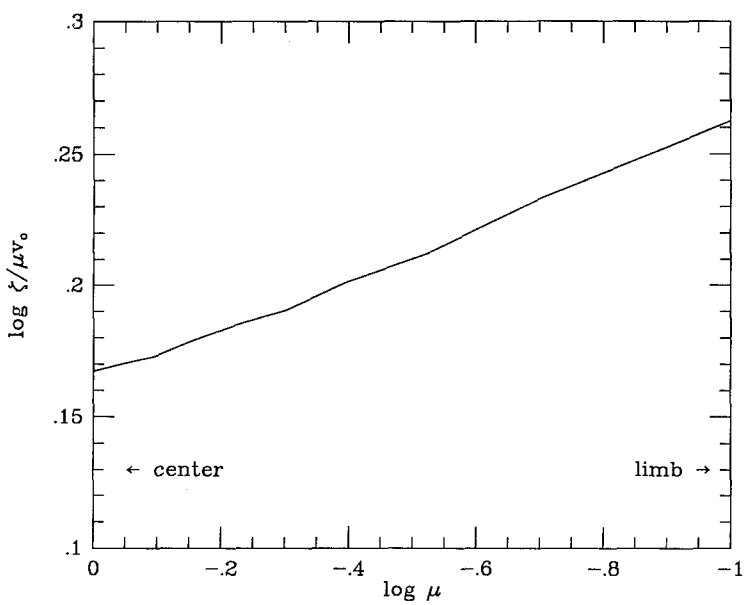

Fig. 5. Center-to-limb variation of Fourier-shift velocity, ζ.

outwardly increasing oscillatory velocity and the shifting of velocity sensitivity to greater heights near the limb as shown in Figure 3(a). For the model used here, one can see from Figure 5 that

$$\frac{\zeta}{\mu v_0} \sim \mu^{-0.09} .$$

Presuming that the model of oscillatory velocity used here is representative of solar conditions, this center-to-limb dependence, if uncorrected, will be convolved with the true spatial variation in the projection of the observed velocities onto spherical harmonics. How seriously this affects the spherical harmonic decomposition is not known but is being investigated in the GONG-sponsored 'artificial data project' which seeks to test reduction and analysis algorithms with simulated data.

5.2. Granulation

It is well known that solar granulation affects the shape of solar Fraunhofer lines (see, for example, Keil, 1980a, b; Dravins, Lindegren, and Nordlund, 1981; Marmalino, Roberti, and Severino, 1987). The velocities of rising and sinking convective granular elements are similar in amplitude to the oscillatory velocities examined here but tend to be confined to low photospheric heights. However, when spatially averaged as in the projected GONG instrumentation, the fact that rising elements are hotter and brighter causes both a line asymmetry and a blueward shift of the average profile whose amplitude decreases towards the limb. Although the quasi-LTE model of line formation is not sufficient for a definitive study, an attempt is made here to gain some qualitative insight into the effects of granular convection on the Fourier phase shift of the Ni 6768 Å line.

To this end, spatially averaged response and phase formation functions have been calculated using granular velocity, temperature, and pressure fluctuations from a recent numerical simulation by Steffen (1988, private communication) using techniques reported by Steffen, Ludwig, and Krüss (1989) and Steffen and Muchmore (1988). The granular model is cylindrically symmetric about the vertical axis. To simulate spatial averaging, it is assumed that an infinite number of identical cylinders of radius r ($= 875$ km) are arranged periodically in a closely packed planar geometry whose horizontal planform is shown in Figure 6. In the interstices between cylinders, the average (VAL-C) model is assumed. The geometry of Figure 6 has rectangular periodicity of length $2r$ in the x-direction and $2r\sqrt{3}$ in the y-direction. For simplicity in the following caculations it is assumed that the azimuthal projection of lines of sight through this geometry lie along the x-axis.

At each horizontal position within the cylinder, the vertical distribution of source function is computed from Equation (27) with the vertical optical depth from Equation (3) using the thermodynamic fluctuations from Steffen's model. Rays with a given heliocentric angle are passed through a rectangular grid at $h = 0$ spanning one period in x and y. The horizontal coordinates at the intersections of a given ray with the

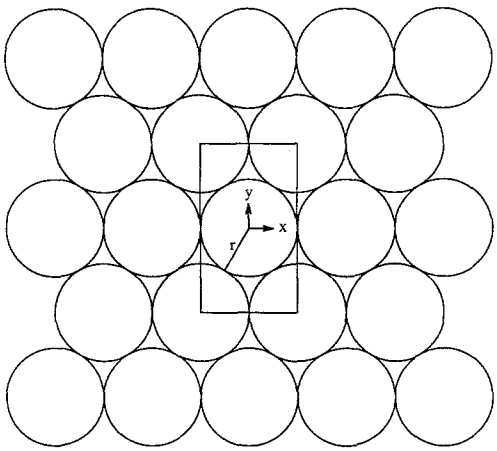

Fig. 6. Section of infinitely repeating horizontal planform for model granulation pattern. Within each circle, the thermodynamic fluctuations and granular velocity fields are taken from Steffen, Ludwig, and Krüss (1989). Between circles, the VAL-C model is assumed. The rectangular box delimits a single two-dimensional period in Cartesian coordinates.

horizontal planes at each height in the model atmosphere grid are determined and values of absorption and emission coefficients are interpolated from Steffen's model and the above '$1\frac{1}{2} - D$' line source function. Using the development of the previous sections, the response and phase formation functions for each ray are calculated and their horizontal averages over one spatial period are reported here.

Spatially-averaged phase formation functions, using laboratory line center as a reference wavenumber and assuming no oscillatory component of velocity, are shown in Figure 7(a) for several values of μ. Within the formation envelope of the Ni line, Figure 7 shows in an average sense the velocity character of Steffen's model, and the decidedly negative (blue-shifted) imbalance in the height distribution shows how the convective limb-shift phenomenon discused above is reflected in the formation of Fourier phase shift. The final shift of the average profile is shown as a function of μ in Figure 7(b) and is compared to recent preliminary measurements by Pierce (1988, private communication). Spectra, averaged over five minutes, were obtained with the Main Spectrograph at the McMath Telescope (NSO/Kitt Peak) with an entrance slit of $\sim 0.5 \times 20$ arc sec; limb shifts were determined from the wavelength position of the central minimum of the line profile. Note that the observations, which were not referenced to an absolute wavelength scale, have been shifted to compare with the calculations at disk center. The rough agreement between the observed and calculated shifts may be fortuitous given the preliminary nature of the data and the many approximations and assumptions inherent in the computations and granulation model but is nonetheless an encouraging sign that the results reported here are reasonably realistic. In any case, Figures 7(a) and 7(b) clearly show that phase formation in the Ni line is sensitive to velocities in height domains where the model granulation cells are quite vigorous and that the limb-shift is a dominant systematic effect in measuring oscillatory velocity fields.

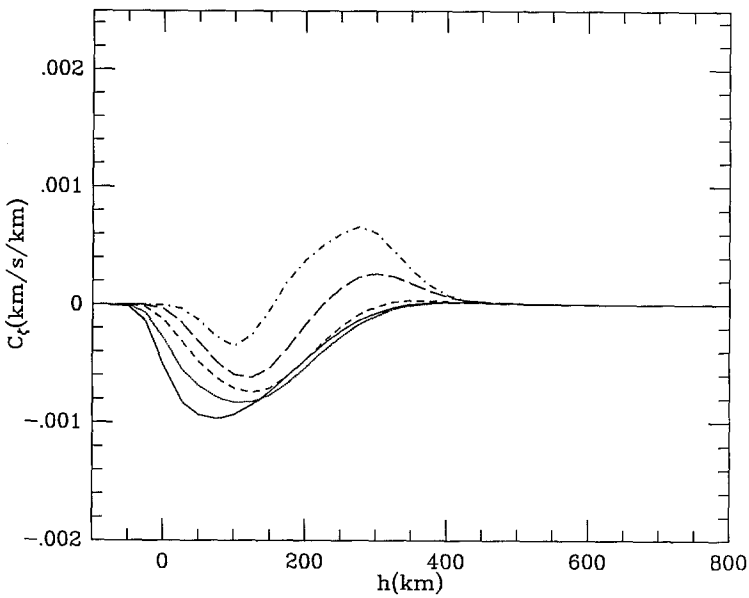

Fig. 7a.

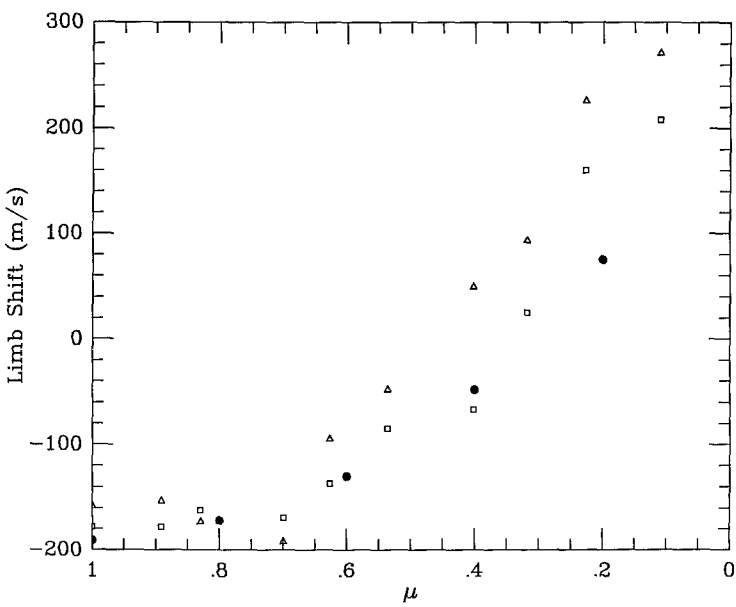

Fig. 7b.

Fig. 7. (a) Horizontally averaged phase formation functions at several values of μ for granulation model with no oscillatory velocity. Line center is referenced to the laboratory frame and dashed patterns are as in Figure 3(a). (b) Model calculations of convective blue shift (solid circles) compared with center-to-limb observations of relative limb shift by Pierce (1988, private communication) in the E–W (open squares) and N–S (open triangles) directions.

In contrast with the dramatic effects of granulation on the phase formation functions, the spatially averaged response functions differ only by $\sim 2\%$ from their non-convective counterparts. This appears to be another consequence of the fact that the response function is nearly independent of total velocity (behavior that extends to the granulation model); the small differences that are present result from the thermodynamic variations across the assumed granulation pattern.

The convectively induced limb-shift phenomenon is of course qualitatively well known and will be 'removed' from helioseismology observations by subtracting a μ-dependent wavelength reference as determined, for example, by time-averages of raw data. To simulate this reduction procedure, phase formation functions including model oscillatory velocities have been computed using the phase shift of the emergent depth profiles for the convective model atmosphere with no oscillatory motion as a μ-dependent wavenumber zero-point. The result for zero, upward, and downward oscillatory motions are shown in Figures 8 and 9. The computed values of ζ differ by $\sim 2\%$ from the non-convective results over the domain of v_0 and μ spanned by the calculations in exactly the same way as the response functions shown above. The differences are apparently now due simply to differences in the average thermodynamic properties of the model atmospheres. Fortunately, the average of the upward and downward shifts (measured with respect to either laboratory or μ-dependent line center) is nearly identical to the result for an atmosphere with zero oscillatory velocity. Thus, in simulation, the effects of the model granulation on measuring the oscillatory velocity can be effectively removed by appropriately referencing the line shifts.

However, Figures 8 and 9 show that this seemingly satisfactory situation is achieved

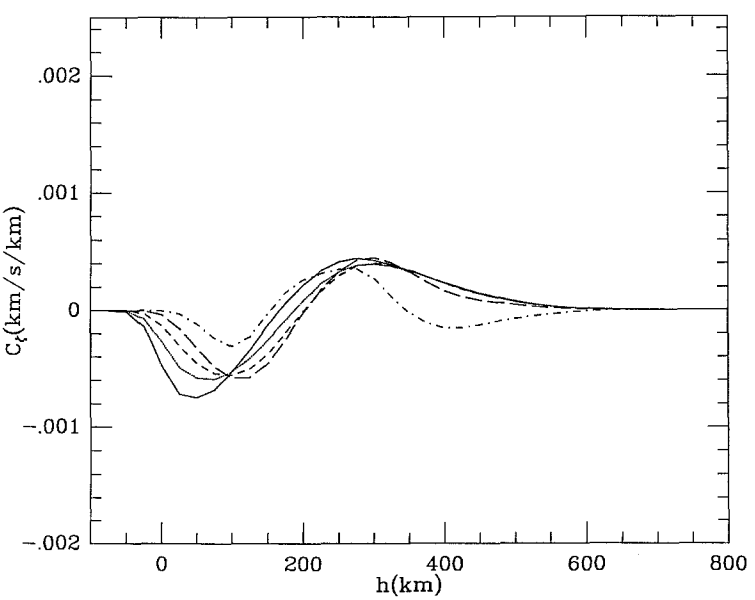

Fig. 8. Horizontally averaged phase formation function for granulation model with no oscillatory velocity, corrected for limb shift (see text). Dashed patterns as in Figure 3(a).

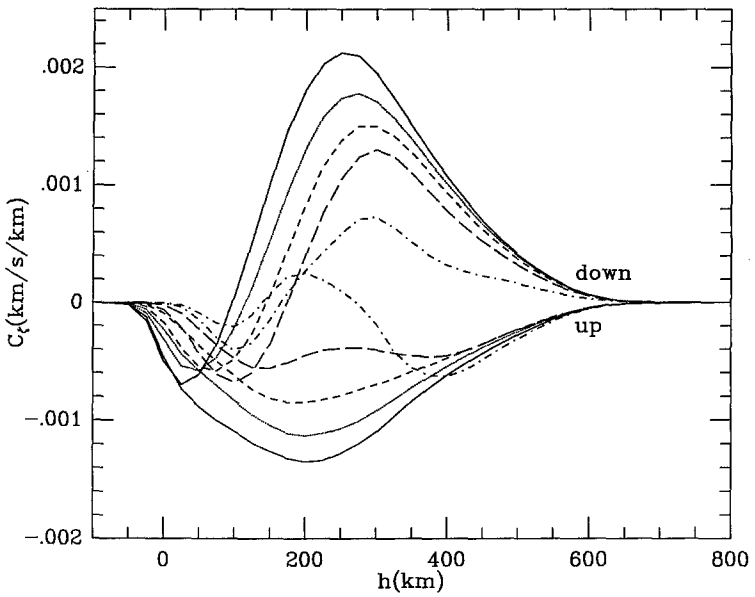

Fig. 9. Horizontally averaged phase formation function for granulation model with upward and downward oscillatory motions, corrected for limb shift. Dashed patterns as in Figure 3(a).

only by a delicate balance between height domains with opposing average senses of convective motion. Moreover, these domains are distributed differently for upward and downward oscillatory motion. Net fluctuations of order one percent in the horizontally averaged flow properties of the granulation model, if uniformly distributed over height, would be sufficient to alter the μ-dependent reference wavelengths by one meter per second.

Granulation on the Sun is a dynamic phenomenon, and both statistical and systematic changes in its thermodynamic and velocity structure with both space and time are either observed or are expected. For example, Miller, Foukal, and Keil (1984) discuss how velocity measurements in selected neutral iron lines are affected by magnetic suppression of convection in supergranule boundaries and suggest that measurements of Doppler wavelength shifts near line center are less subject to confusion from variations in granulation properties. For intermediate-degree helioseismology experiments such as GONG, the most important complication is probably in searching the data for large-scale, quasi-steady flows such as might be associated with 'giant' convective cells. The problem lies less in identifying large-scale convective patterns than with interpreting the results since the thermodynamic and velocity properties of granulation are irrecoverably intermixed in the spatially-averaged Fourier velocity signal.

The interferometric measurement of the phase shift of one component of the Fourier transform of a spectrum line weights intensities at all frequencies in such a way as to produce the highly linear velocity response simulated above. At the same time, it also precludes isolating the core of the line as suggested by Miller *et al.*, although some tuning is theoretically possible by varying the path difference. On these grounds, an ideal line

for Fourier measurements of moderate degree oscillatory modes would be formed higher in the atmosphere than the Ni line. However, many competing instrumental and solar requirements (e.g., the line should be free from telluric blends under a wide variety of atmospheric conditions and from solar blends even in sunspots and near the limb) make the list of possible candidates surprisingly short. Moreover, it is unlikely that any line can be found where the Fourier measurement of velocity fields is entirely free from the influence of granulation. Thus, for the GONG program, the appropriate course is to better understand how to isolate the influence of granulation on velocities inferred from Ni-line data taken with moderate spatial resolution through independent high-resolution observations and further modeling.

6. Summary

In this paper some interpretive tools have been developed for understanding the height-dependence of the formation of Doppler-induced Fourier phase shifts in solar line profiles. In applying the techniques to a simple model of the formation of the Ni I 6768 Å line, three results emerged. First, the Fourier phase is a highly linear measure of velocity even in the presence of velocity gradients and unresolved granular structure. Second, outward increases in oscillatory velocity resulting from the rapidly decreasing density in the photosphere are manifest in a center-to-limb dependence of the corresponding Fourier shifts; higher velocities are inferred near the limb. Finally, the presence of granulation has a profound effect on the formation of the phase shift. Although the simulations reported here suggest that referencing velocity measurements to a μ-dependent zero point determined from time-averaged measurements of the solar 'limb-shift' can accurately compensate for the effects of unresolved *steady state* convection, further observations and more accurate modeling will be needed to separate systematic spatial and temporal variations of granulation from the desired measurements of mass motions.

Qualitatively, the above results are only weakly dependent on the assumed models. However, more accurate modeling is clearly needed, particularly with respect to effects of convection. An important next step is to consider the non-LTE formation of the Ni line more carefully, and the results of Rutten *et al.* (1989) appear promising in this regard. Moreover, more realistic models of the atmosphere, its associated motions, and related spatial and temporal variations need to be included. For example, the possibly important effects of velocity-thermodynamic correlations in the oscillatory motions themselves (see, e.g., Cavallini *et al.*, 1987) have been entirely neglected in this work. Many of the above improvements are planned or are in progress as part of a GONG-sponsored simulation project whose purpose is to study in advance and in as much depth as possible operational and interpretational problems associated with reducing and analyzing future helioseismology data. This study is presented as a step towards that goal.

Acknowledgements

The author wishes to thank T. Brown, T. Duvall, J. Harvey, R. Hubbard, and J. Leibacher for many useful comments and suggestions, M. Steffen for providing computer-readable results from his simulations of granulation, and A. K. Pierce for providing preliminary limb-shift data in advance of publication. This work was partially funded through the NASA Office of Solar and Heliospheric Physics and was carried out at the National Solar Observatory in Tucson, Arizona using computing facilities of the National Optical Astronomy Observatories.

Appendix. Numerical Methods

Given a suitable model atmosphere (including macroscopic velocity) and distributions of population numbers sufficient to compute ε_D and κ along any desired line of sight, one can in principle compute the line depth from Equation (9), the phase formation function from Equation (20), and the velocity response function from Equation (25). The development has been deliberately cast in a form amenable to simple numerical techniques which are discussed in this section.

A1. Optical path length and line profiles

The line-of-sight integration for the formal solution of a transfer equation is effectively performed on an optical path-length scale. In this paper, the absorption coefficient is assumed to have a piecewise exponential variation on a path grid $\{s_1 > s_2 > \ldots > s_L\}$. From Equation (3), the corresponding optical path position evaluated at $2M + 1$ wavenumbers $\{\sigma_0 = 0 < \sigma_1 = -\sigma_{-1} < \sigma_2 = -\sigma_{-2} < \ldots < \sigma_M = -\sigma_{-M}\}$ are

$$\begin{aligned} &\tau_{1,m} = 0\,, \\ &\tau_{l,m} = \tau_{l-1,m} + H_{l,m}[\kappa_{l,m} - \kappa_{l-1,m}], \quad l = 2 \ldots L\,, \end{aligned} \tag{A-1}$$

where, for example, $\kappa_{l,m} \equiv \kappa(s_l, \sigma_m)$ and

$$H_{l,m} = [s_{l-1} - s_l]/\ln[\kappa_{l,m}/\kappa_{l-1,m}]\,.$$

By rewriting Equation (9) in terms of an equivalent source function $\mathscr{S} \equiv \varepsilon_D/\kappa$ which is assumed to have a piecewise linear variation with τ, one finds (temporarily suppressing wavenumber dependence)

$$\begin{aligned} &D_L = 0\,, \\ &D_l = e_l D_{l+1} + [1 - d_l]\mathscr{S}_l + [d_l - e_l]\mathscr{S}_{l+1}\,, \quad l = L - 1 \ldots 1\,, \end{aligned} \tag{A-2}$$

where $e_l = \exp(\tau_l - \tau_{l+1})$ and $d_l = (1 - e_l)/(\tau_{l+1} - \tau_l)$. Series expansions for the coefficients of $\mathscr{S}_l$ and $\mathscr{S}_{l+1}$ are used for small optical intervals. For the models in this paper τ_L is sufficiently large even in the continuum that beginning the calculation with $D_L = 0$ in Equation (A-2) rather than some value based on asymptotic behavior of the source function is of little practical consequence. More sophisticated assumptions (e.g.,

see Jones, 1977) about the functional forms of κ and $\mathscr{S}$ can be used to improve smoothness and absolute accuracy, but these make little difference for the present calculations.

A2. Fourier transforms

To compute the single component of the complex transform for a function f, we simply use the finite Fourier transform, i.e.,

$$\tilde{f} = \sum_{-M}^{M} w_m \exp(-2\pi i \sigma_m x) f(\sigma_m) \Delta\sigma \tag{A-3}$$

for a uniform wavenumber separation $\Delta\sigma$; w_m are apodizing weights (cosine bell) to remove residual leakage. For the present computations, there is no compelling need to adopt the more sophisticated time-saving procedures used in fast Fourier transforms.

A3. Contribution functions

Discrete quadratures approximating the formal solution of the transfer equation are more accurately accomplished when the integration variable is first transformed to optical path length and the exponential factor is included specifically as a weight, as in Equation (A-2). On the other hand, geometric path length is the appropriate variable of integration for quadrature representations of integrals of the phase formation function, C_ζ, (Equation (21)) and for interpreting contribution functions as 'density' distributions showing the contribution per unit height of a given differential height domain to the formation of the desired quantity. To allow consistent geometric interpretation of the more accurate quadrature weights of the optical depth representation and to insure consistency of all the internal summation processes in the computations, the following discrete 'change of variables' is employed.

With the same interpolatory approximation for source function with optical depth which was used in Equation (A-2) above, one can write the quadrature approximation for the emergent line depth as

$$D(\infty, \sigma) \simeq \sum_{l=1}^{L} \gamma_l C_{D_l} , \tag{A-4}$$

where

$$\gamma_l = \begin{cases} (1 - d_1)/\kappa_1, & l = 1 , \\ (d_{l-1}/e_{l-1} - d_l)/\kappa_l, & l = 2, \ldots, L-1 , \\ (d_{L-1}/e_{L-1} - 1)/\kappa_L, & l = L . \end{cases} \tag{A-5}$$

The corresponding integration in geometric depth is written here as

$$D(\infty, \sigma) = \int_{-\infty}^{\infty} C_D(s, \sigma)\, \mathrm{d}s \simeq \sum_{l=1}^{L} \overline{C}_{D_l} \Delta s_l , \tag{A-6}$$

where

$$\Delta s_l = \begin{cases} \frac{1}{2}(s_1 - s_2), & l = 1, \\ \frac{1}{2}(s_{l-1} - s_{l+1}), & l = 2, \ldots, L-1, \\ \frac{1}{2}(s_{L-1} - s_L), & l = L. \end{cases} \tag{A-7}$$

C_{D_l} in Equation (A-4) are evaluated as implied by Equation (9). One can obtain the result of Equation (A-4) using the geometric quadrature (A-6) by defining

$$\overline{C}_{D_l} = \gamma_l C_{D_l}/\Delta s_l. \tag{A-8}$$

The quantities $\overline{C}_{D_l}$ are plotted vs height in Figure 2 and are also used to compute the discrete transforms needed in Equation (20) to evaluate the phase formation function, C_ζ. In this way simple geometric depth quadratures of form (A-6) give the same accuracy as optical depth quadratures of form (A-4) and retain their geometric interpretation and normalization.

A4. Response functions

Similarly, the simplest and most accurate quadratures for integrating the transformed response functions needed in Equation (25) to evaluate $R_{\zeta:v}$ involve a change of integration variable which lead to approximations of form

$$\int_{-\infty}^{\infty} \tilde{R}_{D:v}(s, x)\delta v(s)\,\mathrm{d}s \approx \sum_{l=1}^{L} \tilde{r}_l \delta v_l. \tag{A-9}$$

In particular, if one regards the quantity (see Equation (15))

$$\alpha(s) = \sigma_0/c \int_{-\infty}^{\infty} \exp - [2\pi i x\sigma + \tau(s, \sigma)]\frac{\partial D}{\partial \sigma}(s, \sigma)\,\mathrm{d}\sigma \tag{A-10}$$

as the variable of integration in the left-hand side of Equation (A-9), then

$$\int_{-\infty}^{\infty} \tilde{R}_{D:v}(s, x)\delta v(s)\,\mathrm{d}s = \int_{\alpha(-\infty)}^{\alpha(\infty)} \delta v(\alpha)\,\mathrm{d}\alpha. \tag{A-11}$$

If δv is a piecewise linear function of α, the required quadrature coefficients become

$$\tilde{r}_l = \begin{cases} (\alpha_{l+1} - \alpha_l)/2, & l = 1, \\ (\alpha_{l+1} - \alpha_{l-1})/2, & l = 2 \ldots L-1, \\ (\alpha_l - \alpha_{l-1})/2, & l = L. \end{cases} \tag{A-12}$$

A similar trick is used to evaluate $\alpha_l \equiv \alpha(s_l)$. First, however, note that $\exp(-\tau(s, \sigma))$ can be a very rapid function of wavenumber while all the other functions in the integrand

of Equation (A-10) are comparatively well behaved. A better posed arrangement of terms is thus obtained if one first integrates Equation (A-10) by parts so that $\exp(-\tau(\sigma, s))$ can be incorporated into a variable of integration

$$\beta_l(\sigma) = w(\sigma) \exp - [2\pi i \sigma x + \tau(s_l, \sigma)], \tag{A-13}$$

where w is the apodizing function. In analogy with the steps leading to Equation (A-12), one eventually finds quadrature approximations for α_l of form

$$\alpha_l \approx \tfrac{1}{2}\sigma_0 \Delta\sigma/c \left\{ [\beta_{l,\,-M} + \beta_{l,\,1-M}] D_{l,\,-M} - [\beta_{l,\,M-1} + \beta_{l,\,M}] D_{l,\,M} + \right.$$

$$\left. + \sum_{m=1-M}^{M-1} [\beta_{l,\,m-1} - \beta_{l,\,m+1}] D_{l,\,m} \right\}, \tag{A-14}$$

where $\beta_{l,\,m} \equiv \beta_l(\sigma_m)$. For actual computation, the real and imaginary parts of $\beta_{l,\,m}$ and α_l are computed separately using the appropriate trigonometric expansion for $\exp(-2\pi i \sigma x)$. Before changing variables, one needs, in principle, to divide the above integrals over path length and wavenumber into intervals over which the real and imaginary parts of α and β are monotonic so that the relevant functional relationships are single valued. However, so long as the endopoints of each subinterval lie on a grid point, the quadrature formulae are unchanged, and, in practice, the grids used here are fine enough to resolve this segmentation without serious error.

The explicit formulae for the quadrature equivalents of the response function were derived without recourse to sophisticated representation of integrands. Experience has shown that the seeming indirection leading to Equations (A-12)–(A-14) is well justified by the resulting efficiency and stability which allow meaningful computations with quite modest grids. As in the preceeding section, the real and imaginary parts of $\tilde{r}_l/\Delta s_l$ are used in Equation (25) in place of $\tilde{R}_{D\,:\,v}(s_l, x)$ so that the resulting quantities $R_\zeta(s_l, x)$ which are plotted in Figure 3(a) are normalized to unit geometric length while sums of form

$$\sum_{l=1}^{L} R_\zeta(s_l, x) \delta v_l \Delta s_l .$$

are numerically identical to Equation (A-9).

References

Allen, C. W.: 1974, *Astrophysical Quantities*, The Athlone Press, London.

Beckers, J. M. and Milkey, R. W.: 1975, *Solar Phys.* **43**, 289.

Bracewell, R. N.: 1986, *The Fourier Transform and Its Applications*, second ed., McGraw-Hill, New York.

Brault, J. W. and White, O. R.: 1971, *Astron. Astrophys.* **13**, 169.

Brown, T. R.: 1984, in R. Ulrich (ed.), *Proceedings, Snowmass Conference on Solar Seismology from Space*, Jet Propulsion Laboratory, Pasadena, CA, p. 157.

Caccin, R., Gomez, M. T., Marmalino, C., and Severino, G.: 1977, *Aston. Astrophys.* **54**, 227.

Cavallini, F., Ceppatelli, G., Righini, A., and Alamahni, N.: 1987, *Astron. Astrophys.* **173**, 161.

Corliss, C. H. and Bozman, W. R.: 1962, *Experimental Transition Probabilities for Spectral Lines of Seventy Elements*, National Bureau of Standards Monograph 53.

Dravins, D., Lindegren, L., and Nordlund, A.: 1981, *Astron. Astrophys.* **96**, 345.

Evans, J. W.: 1980, in R. Dunn (ed.), *Solar Instrumentation: What's Next?*, Sacramento Peak Observatory, Sunspot, NM, p. 155.
Jones, H. P.: 1977, *J. Quant. Spectr. Rad. Trans.* **17**, 765.
Jones, H. P.: 1985, *Australian J. Phys.* **38**, 919.
Jones, H. P.: 1987, in *The 1987 Artificial Data Workshop*, Global Oscillation Network Group Report Number 5, National Solar Observatory, Tucson, AZ, p. 13.
Keil, S. L.: 1980a, *Astrophys. J.* **237**, 1024.
Keil, S. L.: 1980b, *Astrophys. J.* **237**, 1035.
Libbrecht, K. G.: 1988, *Space Sci. Rev.* **47**, 275.
Magain, P.: 1986, *Astron. Astrophys.* **163**, 135.
Marmalino, C., Roberti, G., and Severino, G.: 1987, *Solar Phys.* **108**, 21.
Mein, P.: 1966, *Ann. Astrophys.* **29**, 153.
Mihalas, D.: 1978, *Stellar Atmospheres*, W. H. Freeman and Co., San Francisco.
Miller, P., Foukal, P., and Keil, S.: 1984, *Solar Phys.* **92**, 33.
Moore, C. E.: 1959, *A Multiplet Table of Astrophysical Interest*, National Bureau of Standards Technical Note 36.
Rutten, R. J., Bruls, J. H. M. J., Gomez, M. T., and Severino, G.: 1989, *Proceedings, Seismology of the Sun and Sun-Like Stars* (in press).
Steffen, M. and Muchmore, D.: 1988, *Astron. Astrophys.* **193**, 281.
Steffen, M., Ludwig, H.-G., and Krüss, A.: 1989, *Astron. Astrophys.* (in press).
Vernazza, J. E., Avrett, E. H., and Loeser, R.: 1981, *Astrophys. J. Suppl.* **45**, 635.
Wiese, W. L., and Martin, G. A. 1980: in *Wavelengths and Transition Probabilities for Atoms and Atomic Ions*, NSRDS-NBS 68, National Bureau of Standards.